

Article

# Effects of Chloride Ions and Nitrate Ions on the Anodic Dissolution of Iron in Sulfuric Acid Solution

Yongyan Zhu <sup>1,2,\*</sup>, Jianli Zhang <sup>3</sup>, Chao Wang <sup>1,2</sup>  and Liang Li <sup>1,2</sup>

<sup>1</sup> Key Laboratory of Green Synthetic Chemistry for Functional Materials, Jiangsu Normal University, Xuzhou 221116, China; wangc@jsnu.edu.cn (C.W.); lil@jsnu.edu.cn (L.L.)

<sup>2</sup> School of Chemistry and Materials Science, Jiangsu Normal University, Xuzhou 221116, China

<sup>3</sup> Jiangsu Zhongneng Silicon Industry Technology Development Co., Ltd., Xuzhou 221116, China; xsdzhangjl@126.com

\* Correspondence: zhuyongyan@jsnu.edu.cn; Tel.: +86-136-8510-3502

Received: 16 July 2020; Accepted: 11 August 2020; Published: 20 August 2020



**Abstract:** In this paper, the flow injection (FI) technique combined with a partially-closed electrode (PCE) was used to manipulate the physicochemical microenvironment at the electrode/electrolyte interface so as to study the effects of chloride ions ( $\text{Cl}^-$  ions) and nitrate ions ( $\text{NO}_3^-$  ions) on the anodic dissolution of the  $\text{Fe}/0.5 \text{ mol dm}^{-3} \text{ H}_2\text{SO}_4$  system. The anodic dissolution is modified by injecting various composition-containing solutions into the vicinity of the PCE, and then, the electrodisolution processes are analyzed by comparing the  $j$ - $t$  curves before and after the injections. At the initial stage of the passive region, it is found that  $\text{NO}_3^-$  ions promote the anodic dissolution of iron by creating more active sites on the surface of the electrode when  $C_{\text{NO}_3^-}/C_{\text{Cl}^-} = 1:1$ ; however, they inhibit the anodic dissolution by making the film more compact for the strong oxidized characteristics of  $\text{NO}_3^-$  ions when  $C_{\text{NO}_3^-}/C_{\text{Cl}^-} = 10:1$ .

**Keywords:** flow injection; current oscillations; partially-closed electrode; pitting corrosion; chloride corrosion; nitrate corrosion

## 1. Introduction

Pitting may cause tremendous losses and damages for its unpredictable nature and rapid propagation. Chloride ions ( $\text{Cl}^-$  ions) usually induce pitting by breaking down the passive film for its aggressiveness to metallic materials [1–10], so the study on the mechanisms of chloride corrosion is of theoretical and practical significance.

Many reports of the pitting induced by  $\text{Cl}^-$  ions have been documented and several models have already been developed, such as the adsorption theory by Uhlig [11], the point defect model (PDM) by Macdonald [12] and the electric breakdown theory by Szklarska-Smialowska [13]. However, there are still many controversies about the cause, the mechanism and the influencing factors of chloride pitting.

Since  $\text{Cl}^-$  ions and other ions often coexist in the corrosive environment, and it is necessary to study the combined effects of possibly coexisting ions on the corrosion processes of metals [14–21]. In particular, the interaction between  $\text{Cl}^-$  ions and nitrate ions ( $\text{NO}_3^-$  ions) is one of the most complex issues and has already been studied by many researchers [16–21]. In most literatures [17–21], nitrate is used as a corrosion inhibitor. Leckie et al. [14] suggested that the inhibitive effects of  $\text{NO}_3^-$  ions on the corrosion induced by  $\text{Cl}^-$  ions could be explained by the competitive adsorption theory. Newman et al. [15] proposed that the reduction in  $\text{NO}_3^-$  ions on the electrode surface consumed acid and increased the pH value of the electrolyte at the electrode/electrolyte interface, which would make the passivation of the stainless steel easier. Sazou et al. [16] suggested that  $\text{NO}_3^-$  ions at low concentrations promoted the pitting induced by  $\text{Cl}^-$  ions but inhibited it at higher concentrations.

Ma et al. [17] proposed that  $\text{NO}_3^-$  ions were a powerful passivating agent and could inhibit the pitting induced by  $\text{Cl}^-$  ions. Fujioka et al. [18] reported that  $\text{NO}_3^-$  ions could not suppress pit nucleation but could inhibit pit growth slightly. Therefore, due to the complexity of the research system and the diversity of the research methods and approaches, the interaction between  $\text{NO}_3^-$  ions and  $\text{Cl}^-$  ions needs more research.

The physicochemical microenvironment at the electrode/electrolyte interface, such as the concentration of the species, is very important to the electrochemical reactions. The present research adopts a different experimental approach to obtain a deeper insight into the co-effects of  $\text{NO}_3^-$  ions and  $\text{Cl}^-$  ions: a partially-closed electrode (PCE) is set up [22], whose physicochemical microenvironment can be manipulated with the flow injection (FI) of different solutions, so as to obtain more information about the composition and the stability of the passive film on the electrode surface, the anodic dissolution of the electrode, the effects of the injections and so on.

The flow injection technique, which can precisely control the quantity and the speed of the injected solution, is a useful technique for various analyses, such as the detection of DNA fragment, trace level of Fe, Cr, Hg, chloride and so on [23,24]. In the present paper, during the anodic dissolution processes of the  $\text{Fe}/0.5 \text{ mol dm}^{-3} \text{ H}_2\text{SO}_4$  system, a small amount of  $\text{NO}_3^-$  ion and/or  $\text{Cl}^-$  ion containing solution was injected into the vicinity of PCE with FI, which will change the physicochemical microenvironment at the interface. The changes of the  $j$ - $t$  curves before and after the designed disturbance were analyzed; thus, the effects of  $\text{NO}_3^-$  ions and  $\text{Cl}^-$  ions on the anodic processes were obtained with more exact details.

## 2. Materials and Methods

Sketch of the experiment setup with the FI and the PCE is shown in Figure 1. A three-electrode system was used in the electrochemical measurements. As shown in Figure 1, the working electrode was placed in a PMMA (polymethyl methacrylate) tube, whose length and diameter were both 4 mm. Thus, a partially-closed environment was created. There was a hole on the side wall of the tube near the working electrode to place the reference electrode. The hole in the upper part of the tube wall connected the FI device. The volume of the injections could be controlled quantitatively by setting the speed and the duration of the rotations.

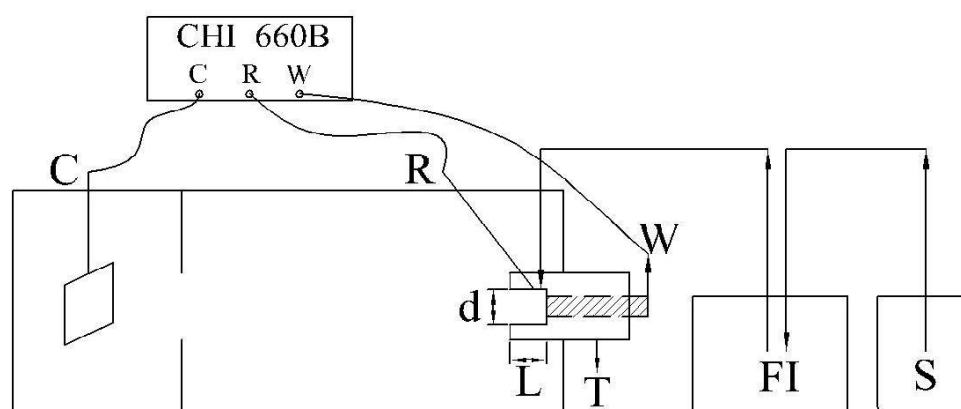


**Figure 1.** Schema of the experimental setup with the flow injection and the partially-closed electrode; S— injection solution; FI—flow injection; W—working electrode (iron or nickel,  $d = 2 \text{ mm}$ ); R—reference electrode (SCE); C—counter-electrode (Pt sheet); T—PMMA tube for the partially-closed electrode (PCE, in which  $L = 4 \text{ mm}$  and  $d = 4 \text{ mm}$ ).

The iron electrode with a diameter of 2 mm (99.99%, Johnson Matthey Company, London, England) was sealed with epoxy resin in a PMMA cylinder, leaving only the end of the rod exposed to the solution. Before each experiment, the specimen was abraded to mirror-like brightness with a series of wet sand paper of different grit sizes (600, 1200 and 2000), and then cleaned successively in an

ultrasonic bath by ethanol and deionized water for 3 min each. The counter-electrode was a platinum plate. The reference electrode was a saturated calomel electrode (SCE) connected to the working electrode by a Luggin capillary in order to minimize the  $iR$  potential drop. All potentials reported here are with respect to SCE. The details of the experimental setup can also be found in our previous publication [22].

The electrochemical measurements were carried out by CHI 660B analyzer (Shanghai Chenhua Instruments Co., Ltd., Shanghai, China) at room temperature. The solutions were injected by a peristaltic pump (Model BT00-600 M, Baoding Lange constant flow pumps Co., Ltd., Baoding, China). The surface morphologies after corrosion were observed with a scanning electron microscope (SEM, Model S-3400N, produced by Hitachi Company, Tokyo, Japan). All these solutions were prepared with analytical grade reagents and deionized water.

Before each electrochemical measurement, the working electrode was immersed in the electrolyte for 10 min. The cyclic voltammetry curves were measured in various solutions from  $-0.5$  to  $1.6$  V, and then scanned in reverse to  $-0.5$  V at the rate of  $10 \text{ mV}\cdot\text{s}^{-1}$ . At 100 s of the potentiostatic polarization, a  $0.037 \text{ mL}$  solution containing  $\text{NO}_3^-$  ions and/or  $\text{Cl}^-$  ions was injected into the vicinity of PCE for 2 s each time, which changed the microenvironment at the electrode/electrolyte interface.

### 3. Results

#### 3.1. Effects of $\text{NO}_3^-$ Ions and/or $\text{Cl}^-$ Ions on the Cyclic Voltammetry Curves

The  $j$ - $E$  polarization curve of the  $\text{Fe}/0.5 \text{ mol dm}^{-3} \text{ H}_2\text{SO}_4$  system, shown in Figure 2A, can be roughly divided into four regions. In the active region (I), the current increased rapidly, and the electrochemical process was mainly controlled by the electron transfer step. In the limiting current region (II), the current remained almost unchanged due to the equal rates for the formation and the dissolution of the surface film, in which the corrosion process was mainly controlled by the mass transfer step. The oscillatory region (III) was an active-passive transition region, and a relaxation type of current oscillations was observed if the potential was constantly controlled at  $E < E_F$  (the Flade potential). In the passive region (IV), the current was low and stable due to a protective passive film formed on the surface of the electrode.

As shown in Figure 2B,C, when there were only  $\text{NO}_3^-$  ions in the solution, the  $E_{pp}$  shifted to the negative direction as the concentration of  $\text{NO}_3^-$  ions increased (Table 1). This phenomenon is related to the redox reaction between  $\text{NO}_3^-$  ions and  $\text{Fe}^{2+}$  ions [25,26]. On the one hand, the consumption of  $\text{H}^+$  ions in the oxidation process resulted in the increment in the pH value at the interface, which was beneficial to the formation of the passive film [13]. On the other hand,  $\text{Fe(II)}$  in the  $\text{Fe(OH)}_2$  film changed into  $\text{Fe(III)}$ , which increased the ratio of  $C_{\text{Fe}^{3+}}/C_{\text{Fe}^{2+}}$  and caused the electrode to passivate more easily [27]. If the solution contained  $\text{Cl}^-$  ions exclusively (Figure 2A'), the passive region did not appear, and aperiodic current oscillations occurred during the backward potential scan, indicating that the pits are induced by  $\text{Cl}^-$  ions [28]. When there were both  $\text{NO}_3^-$  ions and  $\text{Cl}^-$  ions in the solutions, the polarization behavior was dependent on the concentration ratio. If  $C_{\text{NO}_3^-}/C_{\text{Cl}^-} = 1:1$ , the passive region was not observed either; moreover, the curve was smooth and no current oscillations appeared during the polarization process (Figure 2B'). In contrast to Figure 2A', if  $C_{\text{NO}_3^-}/C_{\text{Cl}^-} = 10:1$ , the electrode was passivated at a more positive potential (Figure 2C'), indicating that  $\text{NO}_3^-$  ions at high concentration can inhibit the aggressive action of  $\text{Cl}^-$  ions on the passive film to a certain extent.

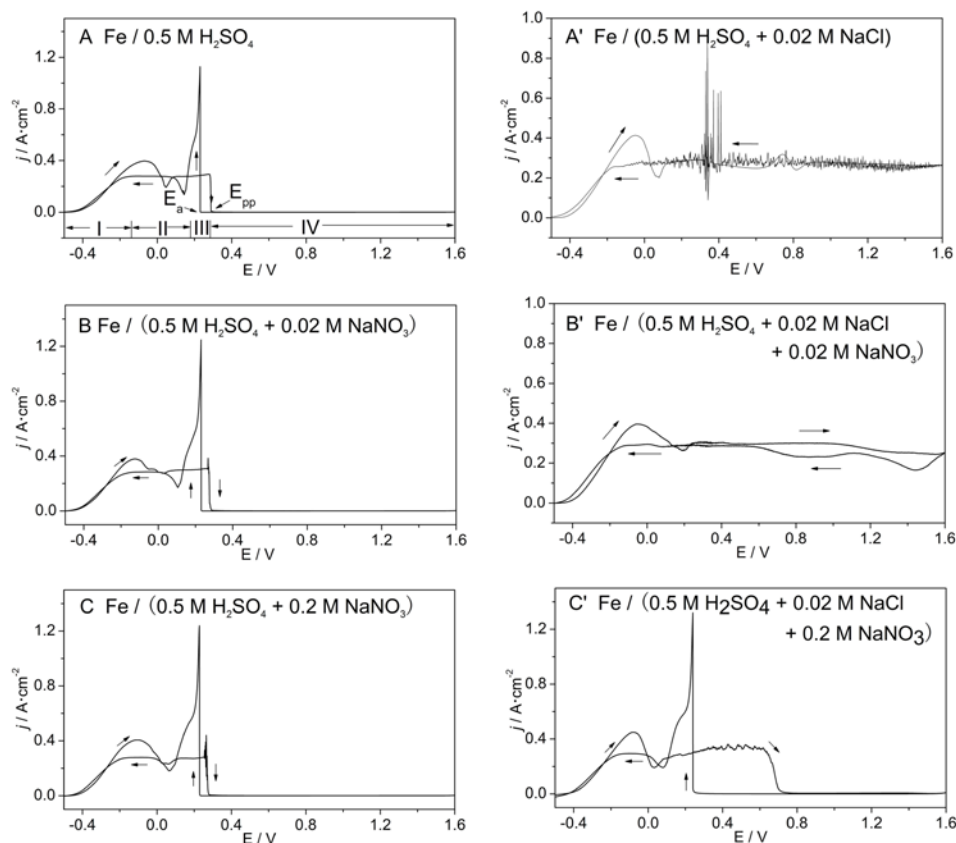


**Figure 2.** The cyclic voltammograms of the iron electrodes at  $dE/dt = 10$  mV/s in various solutions (A) 0.5 M  $H_2SO_4$ ; (A') 0.5 M  $H_2SO_4$  + 0.02 M NaCl; (B) 0.5 M  $H_2SO_4$  + 0.02 M  $NaNO_3$ ; (B') 0.5 M  $H_2SO_4$  + 0.02 M NaCl + 0.02 M  $NaNO_3$ ; (C) 0.5 M  $H_2SO_4$  + 0.2 M  $NaNO_3$ ; (C') 0.5 M  $H_2SO_4$  + 0.02 M NaCl + 0.2 M  $NaNO_3$ .

**Table 1.** Effects of  $NO_3^-$  ions and/or  $Cl^-$  ions on the primary passive potential ( $E_{pp}$ ) in different solutions.

Solutions	$E_{pp}$ (v)	Solutions	$E_{pp}$ (v)
0.5 M $H_2SO_4$	0.289	0.5 M $H_2SO_4$ + 0.02 M NaCl	none
0.5 M $H_2SO_4$ + 0.02 M $NaNO_3$	0.283	0.5 M $H_2SO_4$ + 0.02 M NaCl + 0.02 M $NaNO_3$	none
0.5 M $H_2SO_4$ + 0.2 M $NaNO_3$	0.265	0.5 M $H_2SO_4$ + 0.02 M NaCl + 0.2 M $NaNO_3$	0.720

### 3.2. Effects of $NO_3^-$ Ions and/or $Cl^-$ Ions on the $j-t$ Curves

Figure 3 shows the effects of  $NO_3^-$  ions and/or  $Cl^-$  ions on the  $j-t$  curves at  $E = 0.275$  V. The current was low and stable (Figure 3A) for the passive film on the surface which was dense before the perturbation. As shown in Figure 3B,C, when the injected solutions contained different concentrations of  $NO_3^-$  ions, the current did not change significantly after the injection, indicating the passive films are not destroyed by  $NO_3^-$  ions [29]. However, if there were only  $Cl^-$  ions in the injected solutions, the current oscillations appeared after a period of induction time,  $\tau_0$  (Figure 3A'), which means that the passive film was destroyed by  $Cl^-$  ions; thus, pitting was induced [28]. When the injected solutions contained both  $NO_3^-$  ions and  $Cl^-$  ions, the experimental results changed with the ratio of  $C_{NO_3^-}/C_{Cl^-}$ . If  $C_{NO_3^-}/C_{Cl^-} = 1:1$ , the current oscillations appeared as before (Figure 3B'), but the oscillatory frequency increased, and the induction time reduced ( $\tau_1 < \tau_0$ ) obviously, suggesting that  $NO_3^-$  ions at low concentration assists  $Cl^-$  ions to destroy the passive film. If  $C_{NO_3^-}/C_{Cl^-} = 10:1$ , no oscillation was observed, and the electrode remained passive after the injection (Figure 3C'), indicating that  $NO_3^-$  ions at high concentrations suppress the aggressive action of  $Cl^-$  ions.

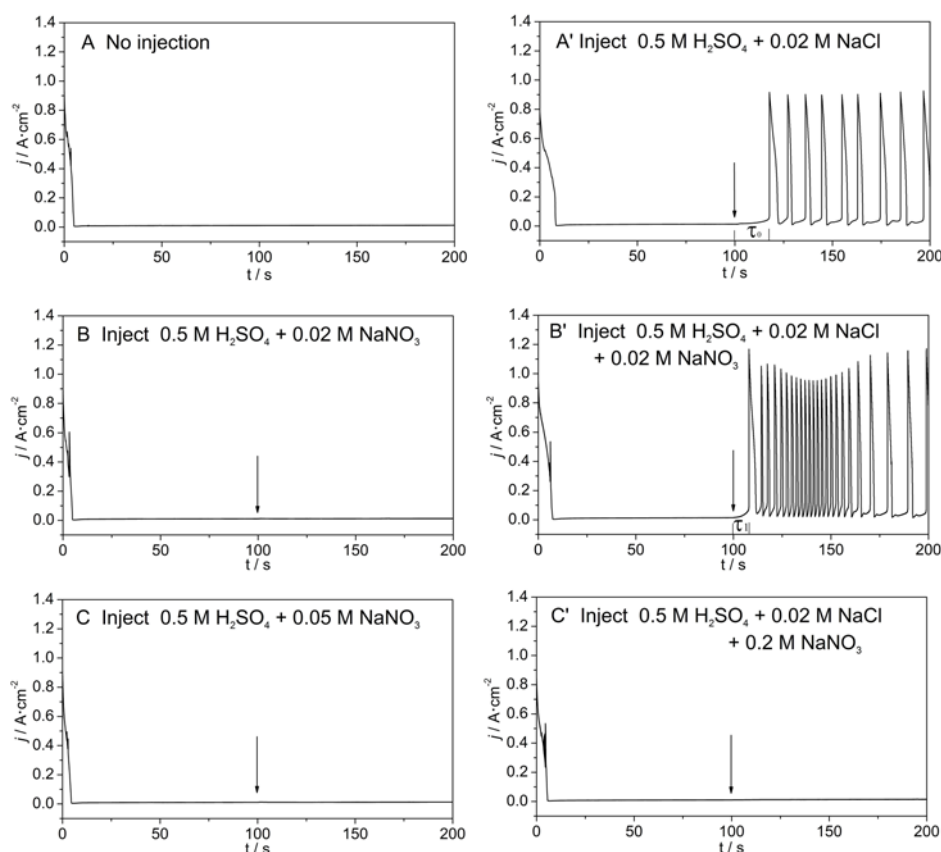


**Figure 3.** Effects of different injected solutions on the  $j$ - $t$  curves of the Fe/0.5 M H<sub>2</sub>SO<sub>4</sub> system at  $E = 0.275$  V (0.037 mL different solutions injected at 100 s) (A) no injection; (A') 0.5 M H<sub>2</sub>SO<sub>4</sub> + 0.02 M NaCl; (B) 0.5 M H<sub>2</sub>SO<sub>4</sub> + 0.02 M NaNO<sub>3</sub>; (B') 0.5 M H<sub>2</sub>SO<sub>4</sub> + 0.02 M NaCl + 0.02 M NaNO<sub>3</sub>; (C) 0.5 M H<sub>2</sub>SO<sub>4</sub> + 0.2 M NaNO<sub>3</sub>; (C') 0.5 M H<sub>2</sub>SO<sub>4</sub> + 0.02 M NaCl + 0.2 M NaNO<sub>3</sub>.

To present the results more clearly, the integral quantity (C) within 100 s after the injections was calculated. The values are presented in Table 2. Obviously, compared with the injected solution only containing Cl<sup>-</sup> ions, the quantity increased when the ratio of C<sub>NO<sub>3</sub><sup>-</sup></sub>/C<sub>Cl<sup>-</sup></sub> was 1:1, but it decreased when the ratio was raised to 10:1. These results consolidate those of the electrochemical curves (Figures 2 and 3).

**Table 2.** The integral electrical quantity after the injection (the integral time is 100–200 s).

Corresponding Curves	Injection Solutions	Coulomb (C)
Figure 2A'	0.5 M H <sub>2</sub> SO <sub>4</sub> + 0.02 M NaCl	0.568
Figure 2B'	0.5 M H <sub>2</sub> SO <sub>4</sub> + 0.02 M NaCl + 0.02 M NaNO <sub>3</sub>	0.800
Figure 2C'	0.5 M H <sub>2</sub> SO <sub>4</sub> + 0.02 M NaCl + 0.2 M NaNO <sub>3</sub>	0.041

### 3.3. The Surface Morphologies of Electrodes after 200 s Polarization

Figure 4 exhibits the surface morphologies of electrodes after the potentiostatic polarization. As shown in Figure 4A, relative uniform corrosion morphology was seen without perturbation. Additionally, no visible change of surface morphology was observed when the Cl<sup>-</sup> free solutions were injected into the vicinity of PCE (Figure 4B,C). If the injected solution only contained Cl<sup>-</sup> ions, obvious pits appeared (Figure 4A'). However, in the presence of NO<sub>3</sub><sup>-</sup> ions in the Cl<sup>-</sup>-containing injections, the corrosion behavior was quite different (Figure 4B',C'). If the ratio of C<sub>NO<sub>3</sub><sup>-</sup></sub>/C<sub>Cl<sup>-</sup></sub> was 1:1, the pits with small radii were numerous and generally distributed (Figure 4B'). Both SEM and the

integral quantity results (Table 2) prove that there are synergistic effects between  $\text{Cl}^-$  ions and  $\text{NO}_3^-$  ions when the ratio is 1:1. When the concentration of  $\text{NO}_3^-$  ions was high (Figure 4C'), the surface morphology was similar to that without injection (Figure 4A) or after the perturbation by  $\text{Cl}^-$ -free solutions (Figure 4B,C). So, the chloride pitting was inhibited by  $\text{NO}_3^-$  ions when its concentration was high.

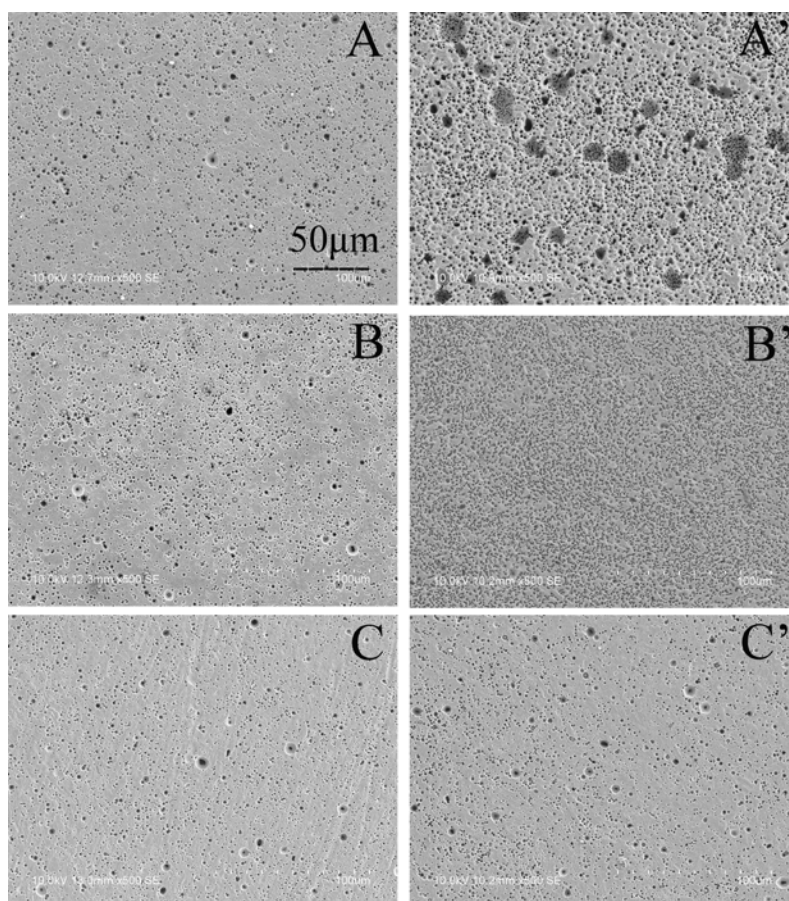


**Figure 4.** The surface morphologies of electrodes after 200 s polarization with injecting different solutions (A) no injection; (A') 0.5 M  $\text{H}_2\text{SO}_4$  + 0.02 M  $\text{NaCl}$ ; (B) 0.5 M  $\text{H}_2\text{SO}_4$  + 0.02 M  $\text{NaNO}_3$ ; (B') 0.5 M  $\text{H}_2\text{SO}_4$  + 0.02 M  $\text{NaCl}$  + 0.02 M  $\text{NaNO}_3$ ; (C) 0.5 M  $\text{H}_2\text{SO}_4$  + 0.2 M  $\text{NaNO}_3$ ; (C') 0.5 M  $\text{H}_2\text{SO}_4$  + 0.02 M  $\text{NaCl}$  + 0.2 M  $\text{NaNO}_3$ .

#### 4. Discussion

Pistorius [30] reported that the pitting induced by  $\text{Cl}^-$  ions can be divided into three successive stages, i.e., pitting nucleation, metastable pitting growth and steady pitting growth. In the following section, the effects of  $\text{NO}_3^-$  ions and  $\text{Cl}^-$  ions on the anodic dissolution of iron are discussed gradually.

If  $C_{\text{NO}_3^-}/C_{\text{Cl}^-} = 1:1$ , the effects of  $\text{NO}_3^-$  ions on the anodic dissolution are as follows.

- (1) As  $\text{NO}_3^-$  ions have strong oxidation characteristics, it will promote the change of  $\text{Fe(II)}$  in the passive film into  $\text{Fe(III)}$  [25,26] (Figure 5A stepI). When  $C_{\text{NO}_3^-} = C_{\text{Cl}^-} = 0.020 \text{ mol dm}^{-3}$  in the same injections, the two anions adsorbed competitively onto the passive film. Thus,  $\text{Fe(III)}$  in the film increases after the injection disturbance.

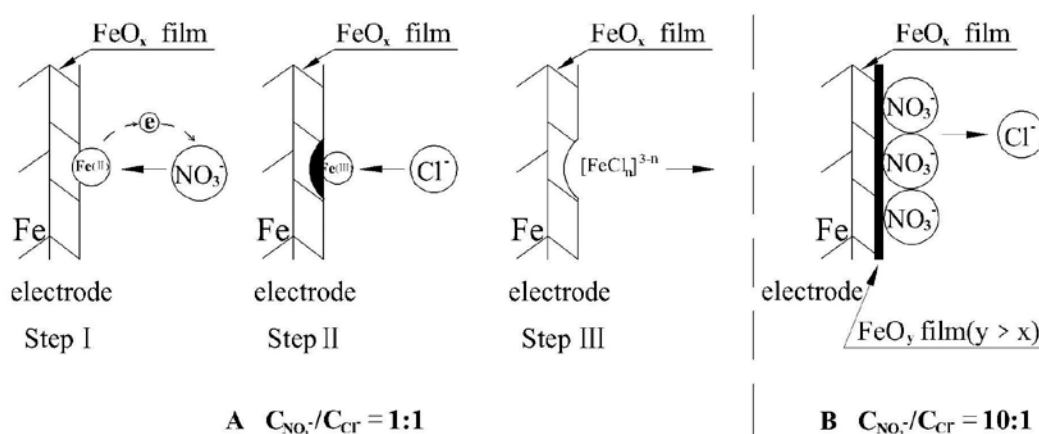


**Figure 5.** Schemata of the effects of  $\text{NO}_3^-$  ions and  $\text{Cl}^-$  ions on the passive film of the iron electrodes (A)  $C_{\text{NO}_3^-}/C_{\text{Cl}^-} = 1:1$ ; (B)  $C_{\text{NO}_3^-}/C_{\text{Cl}^-} = 10:1$ .

- (2) According to the hard and soft acids and bases (HSAB) principle [31], the hard acid  $\text{Fe}^{3+}$  ion combines with the hard base  $\text{Cl}^-$  ion readily. Thus, in the presence of  $\text{Cl}^-$  ions on the electrode surface,  $\text{Fe(III)}$  in the film changes into  $(\text{FeCl}_n)^{3-n}$  and then spreads into the bulk solution quickly (Figure 5A step II and III).

Consequently,  $\text{Fe(III)}$  dispersing in the passive film becomes active/defective sites available for the aggressive action of  $\text{Cl}^-$  ions, which is beneficial for the pits to nucleate. Sazou et al. [7,16,32] and Burstein [33] used the PDM model to explain  $\text{Fe(III)}$  dispersing as the origin of the pits, respectively. Unlike the disturbance by the solution exclusively containing  $\text{Cl}^-$  ions, the active sites for pitting nucleation increase, and their distribution on the surface appears more even, so the current density increases rapidly and the induction time shortens. After the current oscillation is induced, the transformation from  $\text{Fe(OH)}_2$  to  $\text{Fe}_3\text{O}_4$  is accelerated because of the oxidized feature of  $\text{NO}_3^-$  ions, which speeds up the passivation of the electrode. It is verified that the  $E_{\text{pp}}$  is shifted negatively, and the passive film is formed more easily with the increase in the  $C_{\text{NO}_3^-}$  (Table 1). Meanwhile, the film on the surface has just been formed, which is very sensitive to  $\text{Cl}^-$  ions, so the active dissolution is accelerated by the aggressive action of  $\text{Cl}^-$  ions. Since both of the two processes are accelerated, the period of the current oscillation is shortened.

In the pitting growth process, the vast majority of pits disappear after pitting nucleation, and it is difficult to grow into the pitting growth stage. However, according to the above analysis,  $\text{NO}_3^-$  ions at low concentration also possibly favor the metastable pitting growth.

The experimental results of both the electrochemical measurements (Figures 2 and 3) and the SEM morphology (Figure 4) can lead to the conclusion that  $\text{NO}_3^-$  ions at low concentrations facilitate the anodic dissolution of the iron electrode by promoting the pitting nucleation process, and thus accelerates the anodic dissolution.

In comparison, if the concentration of  $\text{NO}_3^-$  ions is higher in the  $\text{Cl}^-$ -containing solution, as shown in Figure 5B, more  $\text{Fe(II)}$  in the passive film changes into  $\text{Fe(III)}$  for the strong oxidized characteristics of  $\text{NO}_3^-$  ions, which make the film compact enough to resist the attack of  $\text{Cl}^-$  ions. At the same time, the opportunities for  $\text{Cl}^-$  ions to adsorb on the electrode surface decrease sharply because there is a competitive adsorption between  $\text{NO}_3^-$  ions and  $\text{Cl}^-$  ions; thus, the concentration of  $\text{Cl}^-$  ions decreases at the interface, and the chances of pitting nucleation induced by  $\text{Cl}^-$  ions reduce as a result. Hence,  $\text{NO}_3^-$  ions at high concentrations inhibit pitting nucleation. Similarly, the self-repairing ability of the system is enhanced as well [17], so the pitting is restrained.

## 5. Conclusions

In this paper, electrochemical measurements are combined with FI and PCE to study the effects of  $\text{NO}_3^-$  ions and  $\text{Cl}^-$  ions on the anodic dissolution of the Fe/0.5 mol  $\text{dm}^{-3}$   $\text{H}_2\text{SO}_4$  system, and the following conclusions can be drawn.

At the initial stage of the passive region,  $\text{NO}_3^-$  ions at low concentrations increase the corrosion rate of iron in the  $\text{Cl}^-$ -containing sulfuric acid solution, because they promote the pitting nucleation by providing more active sites for  $\text{Cl}^-$  ions and also possibly promote the metastable pitting growth by synergistic corrosion of  $\text{NO}_3^-$  ions and  $\text{Cl}^-$  ions, thus accelerating the anodic dissolution; however, at high concentrations,  $\text{NO}_3^-$  ions adsorb competitively with  $\text{Cl}^-$  ions on the electrode surface and their oxidation characteristics (by forming a compact film) inhibit the pitting nucleation and growth, so they inhibit the  $\text{Cl}^-$  ion induced corrosion. At the same time, the experimental results show that the FI technique combined with PCE is an effective method to investigate the corrosion processes of metals.

**Author Contributions:** Conceptualization, Y.Z., C.W. and L.L.; methodology, J.Z., Y.Z., C.W. and L.L.; software, J.Z.; validation, Y.Z., data curation, Y.Z.; writing—original draft preparation, Y.Z.; writing—review and editing, L.L.; supervision, L.L. and C.W.; project administration, Y.Z., All authors have read and agreed to the published version of the manuscript.

**Funding:** This research was funded by the National Natural Science Foundation of China (No. 21303077).

**Acknowledgments:** We would like to thank a Project Funded by the Priority Academic Program Development of Jiangsu Higher Education Institutions.

**Conflicts of Interest:** The authors declare no conflict of interest.

## References

1. Janik-Czachor, M. An assessment of the processes leading to pit nucleation on iron. *J. Electrochem. Soc.* **1981**, *128*, 513C–519C. [[CrossRef](#)]
2. Wang, C.; Chen, S.; Yang, X.; Li, L. Investigation of chloride-induced pitting processes of iron in the  $\text{H}_2\text{SO}_4$  solution by the digital holography. *Electrochem. Commun.* **2004**, *6*, 1009–1015. [[CrossRef](#)]
3. Punckt, C.; Bölscher, M.; Rotermund, H.H.; Mikhailov, A.S.; Organ, L.; Budiansky, N.; Scully, J.R.; Hudson, J.L. Sudden onset of pitting corrosion on stainless steel as a critical phenomenon. *Science* **2004**, *305*, 1133–1136. [[CrossRef](#)]
4. Pagitsas, M.; Pavlidou, M.; Papadopoulou, S.; Sazou, D. Chlorates induce pitting corrosion of iron in sulfuric acid solutions: An analysis based on current oscillations and a point defect model. *Chem. Phys. Lett.* **2007**, *434*, 63–67. [[CrossRef](#)]
5. Lin, B.; Hu, R.; Ye, C.; Li, Y.; Lin, C. A study on the initiation of pitting corrosion in carbon steel in chloride-containing media using scanning electrochemical probes. *Electrochim. Acta* **2010**, *55*, 6542–6545. [[CrossRef](#)]
6. Zimer, A.M.; Rios, E.C.; Mascaro, L.H.; Pereira, E.C. Temporal series micrographs coupled with polarization curves to study pit formation under anodic polarization. *Electrochem. Commun.* **2011**, *13*, 1484–1487. [[CrossRef](#)]
7. Sazou, D.; Pavlidou, M.; Pagitsas, M. Potential oscillations induced by localized corrosion of the passivity on iron in halide containing sulfuric acid media as a probe for a comparative study of the halide effect. *J. Electroanal. Chem.* **2012**, *675*, 54–67. [[CrossRef](#)]
8. Gupta, R.K.; Sukiman, N.L.; Cavanaugh, M.K.; Hinton, B.R.W.; Hutchinson, C.R.; Birbilis, N. Metastable pitting characteristics of aluminium alloys measured using current transients during potentiostatic polarization. *Electrochim. Acta* **2012**, *66*, 245–254. [[CrossRef](#)]
9. Yoon, H.; Ha, H.Y.; Lee, T.H.; Kim, S.D.; Jang, J.H.; Moon, J.; Kang, N. Pitting corrosion resistance and repassivation behavior of C-bearing duplex stainless steel. *Metals* **2019**, *9*, 930. [[CrossRef](#)]
10. Wang, Z.; Gao, Z.; Chu, J.; Qiu, D.; Niu, J. Low temperature sealing process and properties of Kovar alloy to DM305 electronic glass. *Metals* **2020**, *10*, 941. [[CrossRef](#)]
11. Uhlig, H.H. Adsorbed and reaction-product films on metals. *J. Electrochem. Soc.* **1950**, *97*, 215C–220C. [[CrossRef](#)]

12. Macdonald Digby, D. The point defect model for the passive state. *J. Electrochem. Soc.* **1992**, *139*, 3434–3449. [[CrossRef](#)]
13. Szklarska-Smialowska, Z. Mechanism of pit nucleation by electrical breakdown of the passive film. *Corros. Sci.* **2002**, *44*, 1143–1149. [[CrossRef](#)]
14. Leckie, H.P.; Uhlig, H.H. Environmental factors affecting the critical potential for pitting in 18–8 stainless steel. *J. Electrochem. Soc.* **1966**, *113*, 1262–1267. [[CrossRef](#)]
15. Newman, R.C.; Ajjawi, M.A.A. A micro-electrode study of the nitrate effect on pitting of stainless steels. *Corros. Sci.* **1986**, *26*, 1057–1063. [[CrossRef](#)]
16. Sazou, D.; Pagitsas, M. Nitrate ion effect on the passive film breakdown and current oscillations at iron surfaces polarized in chloride-containing sulfuric acid solutions. *Electrochim. Acta* **2002**, *47*, 1567–1578. [[CrossRef](#)]
17. Ma, H.; Yang, C.; Li, G.; Guo, W.; Chen, S.; Luo, J. Influence of nitrate and chloride ions on the corrosion of iron. *Corrosion* **2003**, *59*, 1112–1119. [[CrossRef](#)]
18. Fujioka, E.; Nishihara, H.; Aramaki, K. The inhibition of pit nucleation and growth on the passive surface of iron in a borate buffer solution containing  $\text{Cl}^-$  by oxidizing inhibitors. *Corros. Sci.* **1996**, *38*, 1915–1933. [[CrossRef](#)]
19. Seyedi, M.; Mirjalili, M.; Taji, I.; Armat, O.; Moayed, M. Inhibitive effect of nitrate on pitting corrosion of 17-4ph stainless steel. *Corrosion* **2017**, *73*, 181–191. [[CrossRef](#)]
20. Jegdic, B.; Bobic, B. Pitting corrosion testing of stainless steel AISI 304 in chloride solutions. *Zavar. Zavarene Konstr.* **2015**, *60*, 101–108. [[CrossRef](#)]
21. Street, S.; Xu, W.; Amri, M.; Guo, L.; Glanvill, S.J.M.; Quinn, P.D.; Mosselmans, J.F.W.; Rau, C.; Rayment, T.; Davenport, A. The effect of nitrate on salt layers in pitting corrosion of 304l stainless steel. *J. Electrochem. Soc.* **2015**, *162*, C457–C464. [[CrossRef](#)]
22. Zeng, M.; Wang, C.; Li, L. Designed oscillations of the  $\text{Fe}/\text{H}_2\text{SO}_4$  system with the flow injection in a partially-closed environment. *Electrochem. Commun.* **2009**, *11*, 1888–1891. [[CrossRef](#)]
23. Lannuzel, D.; Jong, J.D.; Schoemann, V.; Trevena, A.; Tison, J.; Chou, L. Development of a sampling and flow injection analysis technique for iron determination in the sea ice environment. *Anal. Chim. Acta* **2006**, *556*, 476–483. [[CrossRef](#)]
24. Fonseca, A.; Raimundo, I.M., Jr.; Rohwedder, J.J.; Ferreira, L.O.S. Construction and evaluation of a flow injection micro-analyser based on urethane-acrylate resin. *Anal. Chim. Acta* **2007**, *603*, 159–166. [[CrossRef](#)]
25. Huang, Y.H.; Zhang, T.C. Effects of low pH on nitrate reduction by iron powder. *Water Res.* **2004**, *38*, 2631–2642. [[CrossRef](#)]
26. Xu, J.; Hao, Z.; Xie, C.; Lv, X.; Yang, Y.; Xu, X. Promotion effect of  $\text{Fe}^{2+}$  and  $\text{Fe}_3\text{O}_4$  on nitrate reduction using zero-valent iron. *Desalination* **2012**, *284*, 9–13. [[CrossRef](#)]
27. Engell, H.J. Stability and breakdown phenomena of passivating films. *Electrochim. Acta* **1977**, *22*, 987–993. [[CrossRef](#)]
28. Sazou, D.; Pagitsas, M. Non-linear dynamics of the passivity breakdown of iron in acidic solutions. *Chaos Solitons Fractals* **2003**, *17*, 505–522. [[CrossRef](#)]
29. Saraby-Reintjes, A. Theory of competitive adsorption and its application to the anodic dissolution of nickel and other iron-group metals—II, The steady state in the prepassive, passive and transpassive potential ranges. *Electrochim. Acta* **1985**, *30*, 403–417. [[CrossRef](#)]
30. Burstein, G.T.; Pistorius, P.C.; Mattin, S.P. The nucleation and growth of corrosion pits on stainless steel. *Corros. Sci.* **1993**, *35*, 57–62. [[CrossRef](#)]
31. Pearson, R.G. Hard and soft acids and bases. *J. Am. Chem. Soc.* **1963**, *85*, 3533–3539. [[CrossRef](#)]
32. Pavlidou, M.; Pagitsas, M.; Sazou, D. Potential oscillations induced by the local breakdown of passive iron in sulfuric acid media. An evaluation of the inhibiting effect of nitrates on iron corrosion. *J. Solid State Electrochem.* **2015**, *19*, 3207–3217. [[CrossRef](#)]
33. Burstein, G.T. Passivity and localized corrosion. *Shreir's Corros* **2010**, *2*, 731–752.

